Chapter 5

Samples and Results

In this thesis several samples were studied. A double layer consisting of a Co wedge and 12 ML of Ni was grown epitaxially on a clean Cu(001) surface (sample A). This sample showed a spin reorientation transition (SRT) from out-of-plane to in-plane with increasing Co thickness [66]. This SRT was due to the competition between the Ni layer having an out-of-plane anisotropy and the Co layer having an in-plane anisotropy energy that increases with its thickness. In the out-of-plane anisotropy region, a reduction of the stripe domain width by a competition of the static magnetic energies was observed upon approaching the SRT. A slow evolution of the magnetic domains upon heating the substrate or upon deposition of more Co is observed in the out-of-plane magnetization region. The experiments have been performed at the Swiss Light Source using an Elmitech PEEM (see Fig. 4.2).

In Sections 5.2 to 5.5, the ns range magnetization reversal in magnetically soft FeNi layers of SV (sample B, C and D) or MTJ (sample E) like trilayer systems is presented, that has been investigated by single-pulse experiments and stroboscopic pump-probe experiments. These experiments were performed at BESSY. The dependence of the reversal on micromagnetic parameters like the coupling energy between two FM layers, the strength of anisotropy energies, the domain wall energies and the stray field from domain walls in the hard Co layer, are investigated.

5.1   Slow magnetization dynamics on a Co/Ni double layer

5.1.1   Sample A

A Co-wedge/12 ML-Ni double layer was grown epitaxially on a clean Cu(001) surface in ultrahigh vacuum (UHV) by molecular beam epitaxy. The clean surface was prepared by the repetition of 1 keV Ar^+ sputtering and annealing the substrate ($\sim$800 K). Two evaporators, Co and Ni, were mounted onto the PEEM UHV chamber, so that the domain structure could be imaged during the film growth. Wedge films were grown by a lateral graduation of the density of Co molecules

(see Fig. 5.1). The sample could also be heated up while taking images. The tungsten filament for heating was mounted at the back of the sample (see Fig. 5.1). Growth rates of Co and Ni were around 8 minutes per ML and 2 minutes per ML, respectively. Using low energy electron microscopy (LEEM), atomic terraces with a maximum width of 500 nm were observed on the clean Cu surface.

Epitaxially grown Ni films on Cu(001) has been studied a lot (see for example Refs. [28,49,66]), because of their unique feature: The Ni film has an out-of-plane anisotropy in a wide thickness range, around between 8 ML to 60 ML, on a Cu(001) surface. By fabrication of the wedge-shaped film with an in-plane anisotropy energy (a Co film in this study) on Ni/Cu(001), where the Ni layer has an out-of-plane anisotropy, a spin reorientation transition (SRT) as a function of Co overlayer thickness can be observed. The SRT is the region where the in-plane anisotropy energy overcomes the out-of-plane one upon increasing the Co thickness, and vice versa. Approaching the SRT from the out-of-plane anisotropy region, a stripe domain structure is often observed, and its domain width gets smaller [49, 67, 68]. The SRT in the crossed-wedge Co/Ni double layer has been studied by Kuch *et al* [66]. At the SRT, the sum of the anisotropy and demagnetizing energies E, will be zero.

$$E(d_{Ni}, d_{Co}) = K_{Ni}(d_{Ni}) + K_{Co}(d_{Co}) - \frac{\mu_0}{2}M^2_{S,Ni} - \frac{\mu_0}{2}M^2_{S,Co} = 0, \tag{5.1}$$

where $K_{Ni}(d_{Ni})$ and $K_{Co}(d_{Co})$ are the anisotropy energies of the Ni and the Co films, each depending on its thickness, d_{Ni} and d_{Co}, respectively. The epitaxially grown films have a volume anisotropy,
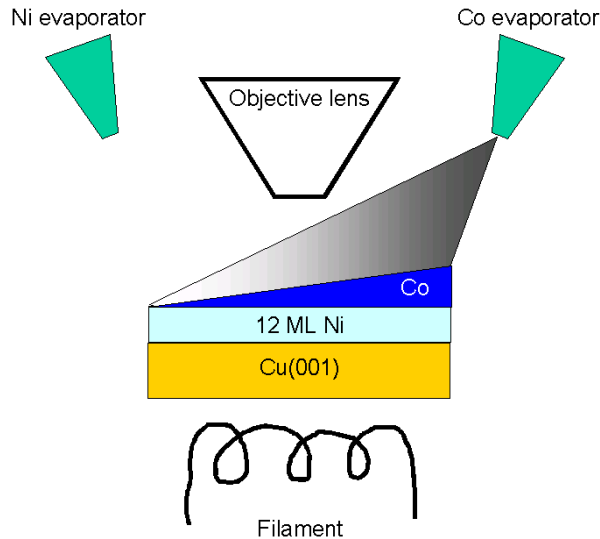

Figure 5.1: Simple diagram of film growth. The evaporators of Ni and Co were mounted directly on the PEEM UHV chamber. The filament for sample heating is located on the back side of the substrate. XMCD-PEEM images could be taken during the film growth and while heating the substrate.

K_V (Section 2.3.2). Since the misfit between the bulk Ni and Cu is only 2.5 % (Ni has a smaller lattice constant), the Ni film does not undergo a reconstruction during its growth. Thus the Ni film is extended in the film plane and compressed in the z direction as a consequence of the tensile stress imposed by the substrate. The total anisotropy energy, K, is a sum of volume and interface anisotropies, $K = K_V + K_S/d$, where d is the film thickness. The demagnetizing energies of the Ni and Co layers are $\mu_0/2\, M_{S,Ni}^2$ and $\mu_0/2\, M_{S,Co}^2$, respectively.

In the perpendicularly magnetized region, a slow magnetization reversal (in the second range) has been observed, in which the driving forces were either the temperature (by heating the sample) or the anisotropy (by growing more Co material). In the former case, the transition from the FM state to the PM state was observed via a reduction of stripe domain width and a splitting of stripe domains, on a purely out-of-plane anisotropy region. In the latter case, the motion of the SRT region by a creeping of stripe domains was observed.

5.1.2 Reduction of magnetic domain size in an ultrathin film

In Fig. 5.2, the magnetic domain structures in the wedge shaped Co layer grown on 12 ML Ni/Cu(001) are shown. The thickness of the Co layer increases from top to bottom. The thickness range of the Co layer is around 2 ML. Fig. 5.2 (b) is the enlarged view of the encircled area in (a). The dark area in (b) indicated by three circles is enlarged, and shown in (c). The upper part in (a), above 0 μm in Y-position, has a pure out-of-plane magnetization. Black and white contrast in this region indicates magnetization pointing out of and into the surface plane, respectively. At the bottom of image (c), the magnetization is in the film plane. The magnetization direction is shown by a white arrow. The stripe domain structure is seen in between, and the width of the stripes decreases upon approaching the in-plane region, i.e., upon increasing the Co thickness. In (c), the end of stripe domain area is seen.

However, the magnetic domain structures between (a) and (b) are a bit different. The stripe domain area is extended into the in-plane anisotropy region in (b) compared with in (a). This is attributed to a surface contamination of the Co layer. A similar effect was observed by Sander *et. al.* [69], who attributed the switching of the easy axis of magnetization from in-plane to out-of-plane of a Ni film deposited on Cu(001) to the absorption of hydrogen on the surface. Images in (b) were taken 30 minutes after the acquisition of the image (a). The Co surface can be contaminated even in UHV (10^{-8} Pa) by the residual gas during that time.

The Co and Ni layers have exactly the same domain structure, because they are in direct contact. This was checked by taking domain images in the same field of view for the Co and Ni layers, for which the photon energies were tuned to the Co-$_3$ and Ni-L$_3$ absorption edges, respectively.

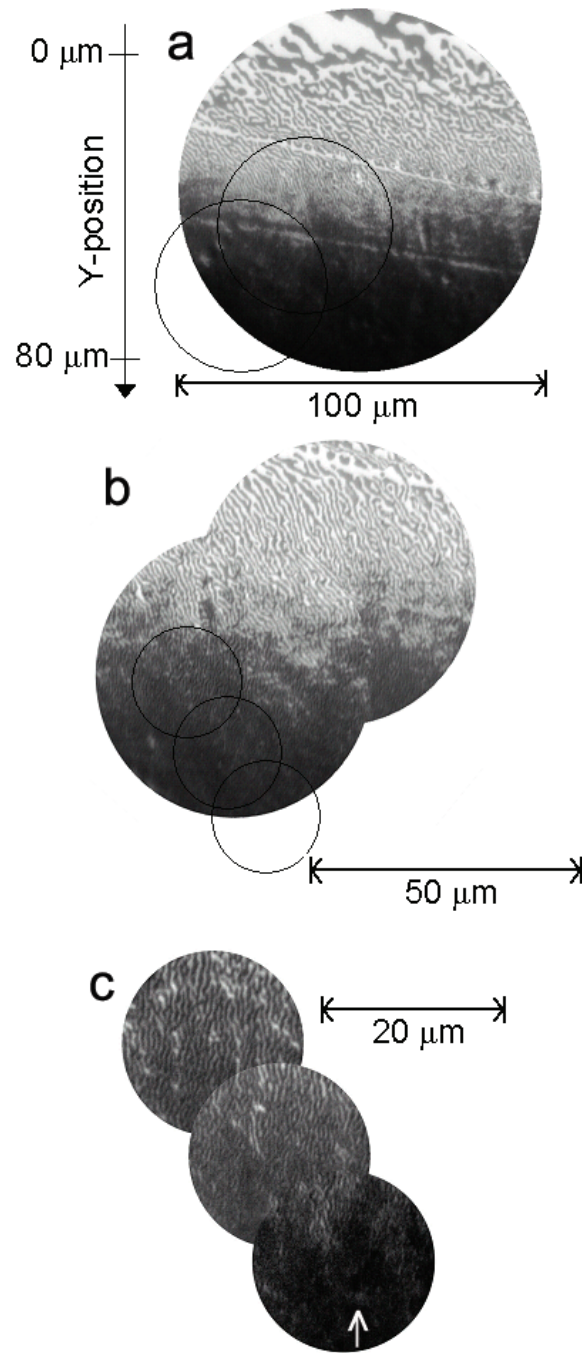From Fig. 5.2, the Z-component of the magnetization, M_Z (a), and the period of the stripe

Figure 5.2: Magnetic domain structure of the wedge-shaped Co layer on a 12 ML Ni/Cu(001) clean surface, obtained by XMCD-PEEM. The photon energy was tuned to the Co-L_3 absorption edge. (c) is a blown up view of (b), and (b) is a blown up view of (a). The upper area in (a) and the bottom area in (c) have out-of-plane and in-plane magnetization directions, respectively. In between, the stripe domains are seen, and their width decreases as the Co thickness increases. The Co thickness increases from top to bottom, in a thickness range around 2 ML.
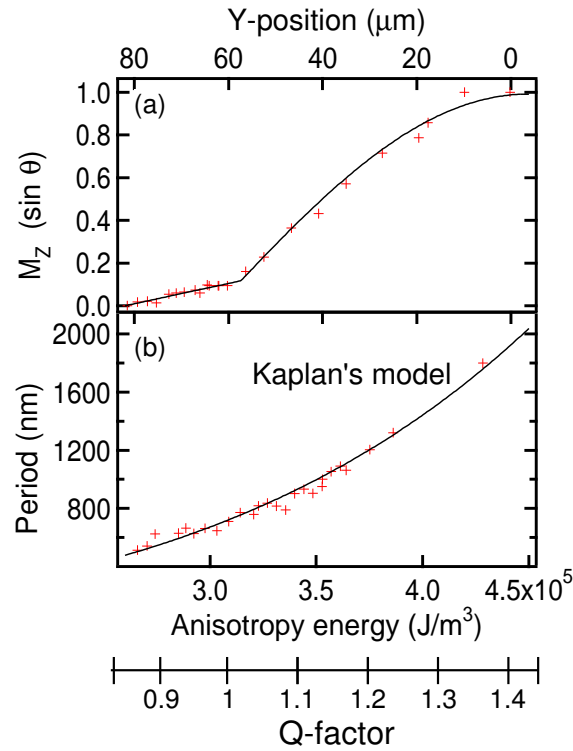
Figure 5.3: (a) M_Z and (b) P are plotted as a function of Y-position, anisotropy energy, and Q-factor. The solid curve in (a) is a guide to the eye. It follows a sine curve at larger polar angle, and is linear for small M_Z. The solid curve in (b) is a fit using Eq. 5.2.
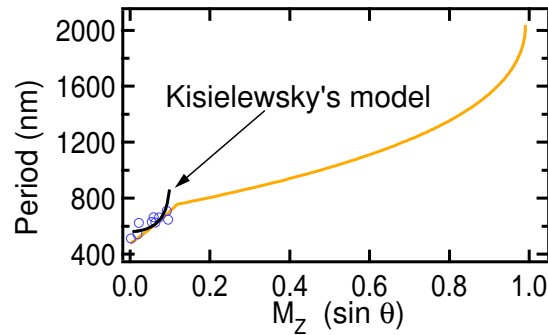

Figure 5.4: P vs. M_Z. The grey solid curve is obtained from the two curves in Fig. 5.3. Experimental data are plotted with circles. At lower M_Z region, the data are fitted with a model derived by Kisielewsky (Eq. 5.3) with $\Theta = 10 \times M_Z$ (black solid curve).

domains P (b) vs. Y-position, anisotropy energy, K, and Q-factor are obtained and shown in Fig. 5.3. The Q-factor indicates the ratio between the anisotropy energy and the demagnetizing energy ($= K/K_d$). In (a), θ is the angle between the magnetization direction and the surface plane. At around 0 μm in Y-position, the width of the domains drastically shrinks and starts to show the stripe domains. At the same point, M_Z starts to decrease, meaning that the spins start to cant. The reduction of M_Z follows a sine law down to 10 degrees from the surface plane. Afterwards, it decreases linearly with Y-position, i.e., linearly with K. Here it was assumed that only K changes as the thickness of the Co layer increases, and not K_d, since the variation of the Co layer thickness is small (less than 1 ML).

Kaplan [38] has suggested that the dependence of the stripe period on the thickness d and the characteristic length l_c, [where $l_c = \gamma_{DW}/2K_d$, and $\gamma_{DW} = 4\sqrt{AK}$ is the wall energy], using the following equation,

$$P = 2d \, \exp(1 + \frac{\pi a}{2} + \frac{\pi l_c}{d}) \quad \text{(Kaplan's model)}, \tag{5.2}$$

where a = –0.666 for $d/l_c \gg 1$ [38]. The exchange constant, A, is fixed to 6.6×10^{-11} J/m, while a bulk Ni and Co have the same order of A. The total K_d for the double layer is $\sim 3.1 \times 10^5$ J/m^3. This is a sum of K_d for 12 ML Ni and 2 ML Co films, 1.4×10^5 J/m^3 and 1.7×10^5 J/m^3, respectively, as taken from Ref. [66]. This fits very good to the data showed by a solid curve in Fig. 5.3 (b), if one assumes a linear relation between Y-position and K. This was used to fix the K and Q-factor scales.

The transition from a stripe domain state to a monodomain state with in-plane magnetization takes place not when the Q-factor is 1, but it is when the Q-factor is slightly lower than 1. It was suggested by Kisielewsky [35] that a line profile of the magnetization perpendicular to the wall in stripe domains shows a sinusoidal modulation below a Q-factor of 1. Because of the limitation of the lateral resolution, it was not really possible to observe the onset of the sinusoidal wall profile. The lateral resolution was around 100 nm. However, it can be assumed that the Q-factor is 1 at around the kink in Fig. 5.3 (a). Below that kink, a slow decrease of M_Z is observed. It is analytically estimated in Ref. [35] that there is a tendency to minimize M_Z by inducing a sinusoidal wall profile. In this region, the variation of P is expressed with

$$P = \frac{2l_{ex}^2 \pi (8(1 - \sqrt{1 - \Theta^2}) + \frac{\Theta^2 d^2}{l_{ex}^2})}{\Theta^2 d} \quad \text{(Kisielewsky's model)}, \tag{5.3}$$

where Θ is an amplitude of wall profile, which is $M_Z \times \theta_0$ (an inverse of the sinusoidal modulator of elliptical integral). A larger number of θ_0 reflects a more squared wall profile. The exchange length, $l_{ex} = \sqrt{A/K_d}$. As M_Z approaches zero, Eq. 5.3 becomes,

$$P_{min} = \frac{8\pi l_{ex}^2}{d} + 2\pi d. \tag{5.4}$$

In Fig. 5.4, P vs. M_Z is plotted. The thick grey line is obtained by comparing the fitting-curves in Fig. 5.3 (a) and (b). In the sinusoidal region, experimental data are plotted with circles and fitted with Eq. 5.3, where $\theta_0 = 10$ was found by fitting. The smallest, P_{min}, obtained here was $\sim$500 nm. A similar P_{min} of $\sim$550 nm is also estimated from Kisielwsky's model (Eq. 5.4).
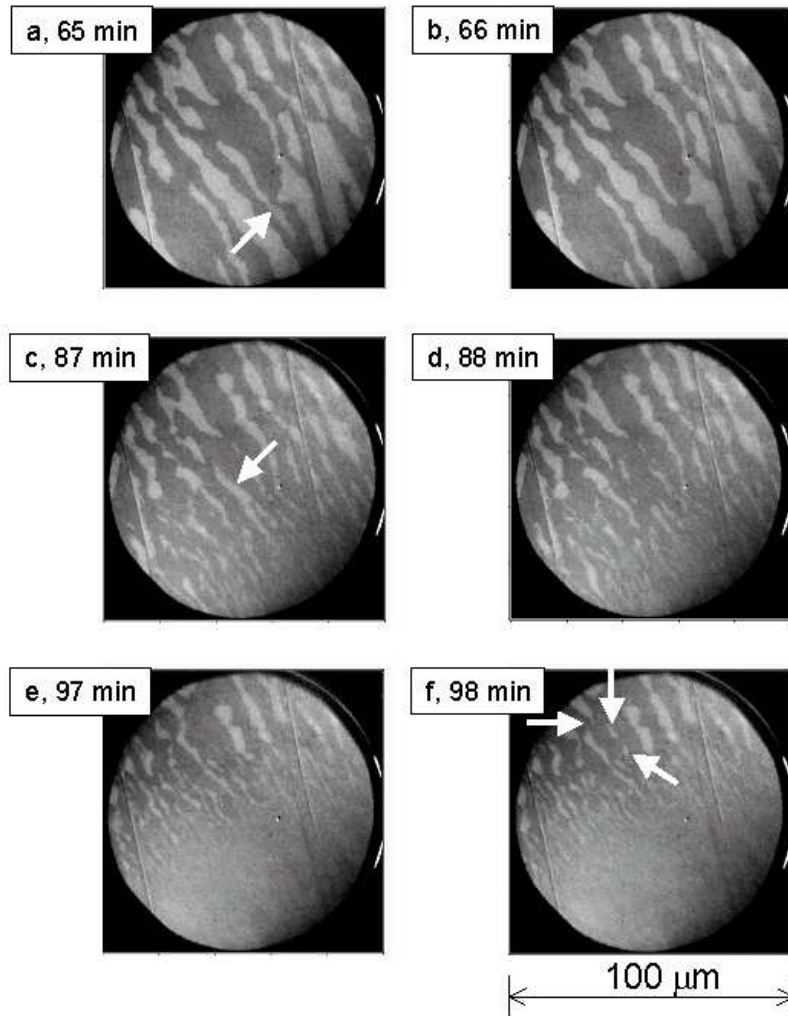

Figure 5.5: Magnetic domain images of a 12 ML Ni film during a slow increase of sample temperature. The evolution of the magnetic domain structure in 1 minute steps from the left image to the right in each low. There seems to be a small variation of the Ni layer thickness over the field of view, it increases slightly from bottom-right to top-left. The PM state appeared at the bottom-right of the images and expanded to top-left.

5.1.3 Wall melting by heating

The field of view was moved to the 100% out-of-plane anisotropy region where no Co was deposited, and the camera exposed images while heating the sample from room temperature to above the Curie temperature of the Ni film. The exposure time of the camera was 32 seconds with 28 seconds delay between exposures, i.e., 1 image per minute. The photon energy was tuned to the Ni-L$_3$ absorption edge (855 eV) with σ^+ polarization. Later on a background image was subtracted from these images, which was taken at a photon energy below the Ni-L$_3$ edge (850 eV) to enhance the magnetic contrast. The temperature increased up to around 430 K in 30 minutes. Afterwards, the heating rate was extremely slow. The thermocouple mounted close to the sample showed that the temperature increased by 1 K in around 30 minutes. The domain wall motion and domain nucleation were observed during the slow heating.

Six out of 120 images are shown in Fig. 5.5. The field of view is 100 μm in diameter. (a) to (b), (c) to (d) and (e) to (f) show the evolution of the domain structure in 1 minute. Image (a) is quite similar to the image before heating. However, one minute later (b), one of the big domains has disappeared, indicated by the white arrow in (a). After 87 minutes, it is seen that the size of the stripe domains got smaller at the bottom-right of the image. One of the events is indicated by the white arrow in (c). A white domain was broken into several smaller ones. In (e), the paramagnetic (PM) region moved into the field of view at the bottom-right. The splitting of domains is also seen going from (e) to (f). Furthermore, nucleation of domains, pointed out by arrows, close to the transition area between the FM and PM regions is also observed.

The thickness of the Ni layer was 12 ML. However, there seems to be a small variation of the thickness over the field of view. It is seen from Fig. 5.5 that the paramagnetic state appeared first at the bottom-right of the images during the heating, and then moved to top-left, i.e., the Ni layer thickness increases from bottom-right to top-left.

5.1.4 Domain wall jumps during deposition

On a wedge-shaped Co film on 12 ML Ni/Cu(001), the motion of the SRT line with jump-like wall motion was observed upon depositing more Co material, where the thickness of the Co layer increases from top-left to bottom right. Since the Co evaporator was mounted on the PEEM chamber, it was possible to take PEEM images during the deposition. The field of view was moved to a region that was top-left of the SRT line, then the camera was started at the same time as the deposition. The camera exposed images for 1 second with zero delay time. The movement of the SRT line was observed from bottom-right to top-left in the field of view. Four out of 462 images of the sequence are shown in Fig. 5.6. The field of view was 50 μm. The upper-left area in the images where the double layer had out-of-plane anisotropy. On the other hand, the bottom-right
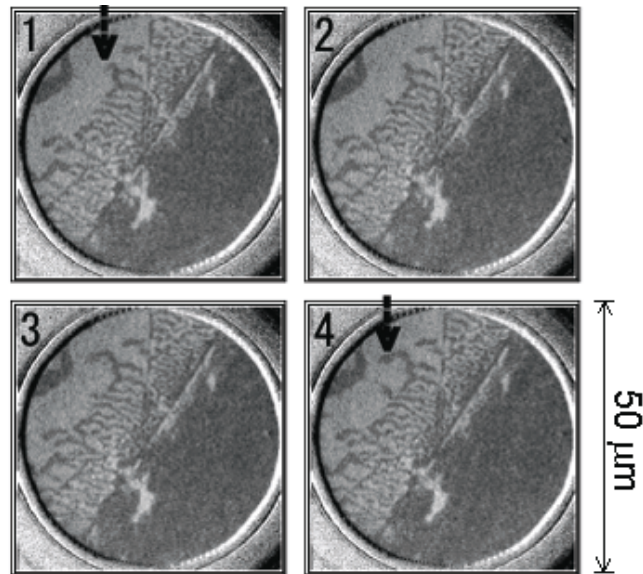
Figure 5.6: Magnetic domain structure in the Co layer on Ni/Cu(001) obtained by XMCD-PEEM during Co deposition, where Ni had perpendicular anisotropy and the Co film was grown as a wedge. The sample area in the top-left part of the images has a pure out-of-plane magnetization, while bottom-right area has in-plane magnetization. In between the stripe domains are visible. Four images from the movie (462 images) are shown. Exposure time was 1 second for each image and with no delay time between images. (a) to (d) were taken at 246, 247, 248 and 249 ns, respectively, after the starting of Co deposition.

area had in-plane anisotropy. Because of the residual field from the magnetic lenses, even though compensated, this area showed a single domain with black contrast. The stripe domains are visible between above two regions, and their width gets smaller approaching the in-plane magnetization region, as described in Section 5.1.2.

In Fig. 5.6, the progress of the SRT line by a creeping motion of stripe domains is seen. One typical motion is indicated by the thick arrows in Fig. 5.6 (1) and (4). For 5 seconds no big motion was observed in this area before (1), then a wall jump has taken place from (2) to (3). After that, no big motion was observed until this domain was surrounded by other stripe domains. Then it was separated into small domains upon depositing more Co. In this experiment, the driving force was the variation of the anisotropy energy upon depositing Co material, and the surface roughness, atomic steps, nm-size scratches hindered the magnetic domain wall motion to immediately assume the stripe domain pattern lowest in energy. This unique magnetization reversal will be discussed in Section 6.2.

5.2 Domain structure evolution by magnetic field pulses

5.2.1 Sample B

The SV-like sample B (Fig. 5.7), 5 nm $Fe_{20}Ni_{80}$/10 nm Cu/5 nm Co capped with 1.5 nm of Au, was grown by molecular beam epitaxy on a step-bunched Si(111) surface. The Si surface was inactivated by a 0.3 nm Cu capping layer. The miscut of the surface was $4°$ along the $[11\bar{2}]$ crystal axis. The substrate surface presents terraces (approximate dimensions 1 μm $\times$ 60 nm with 6 nm height) that are transferred to the magnetic films. The procedure to create step-bunches is the following. The Si(111) surface had a (1×1) surface reconstruction of terraces at high temperature (above 850 °C). Below 850 °C, the (7×7) reconstruction appears. Due to a higher step energy on the (7×7) reconstructed surface, the steps prefer to bunch, leading to a surface made of large flat (7×7) reconstructed terraces separated by bunches of steps. A cross section transmission image of a MTJ like system, 5 nm Al/15 nm FeNi/2 nm Al_2O_3/15 nm Co/0.3 nm Cu on the same substrate, is shown in Fig. 5.8 from Ref. [46]. Steps on the Si surface are seen at the bottom. They are transferred to the magnetic films. As a result, the two FM layers exhibit an in-plane uniaxial anisotropy with the easy axes along the step bunches. The square-shaped Kerr effect loops shown in Fig. 5.10 confirm that the uniaxial anisotropy is along the step-bunches. The periodic modulation of surface roughness causes magnetostatic parallel (Orange peel [70, 71]) coupling. This occurs if the spacer layer thickness is thin compared to the amplitude of the surface/interface corrugations of
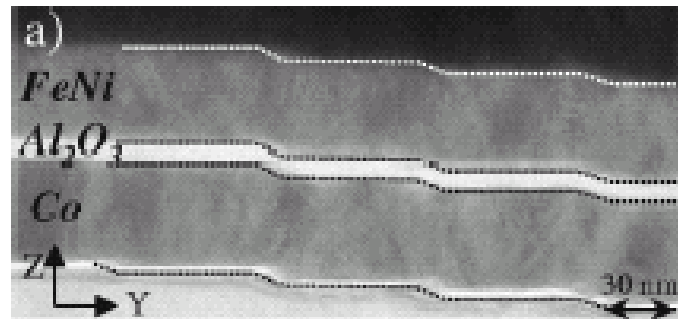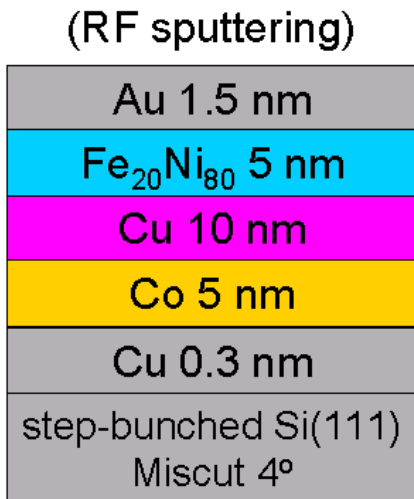

Figure 5.7: Structure of the spin-valve like trilayer system (Sample B). Films were grown on a step-bunched Si(111) surface by Molecular Beam Epitaxy.

Figure 5.8: Cross section image of an MTJ like system, 5 nm Al/15 nm FeNi/2 nm Al_2O_3/15 nm Co/0.3 nm Cu, deposited on step-bunched Si(111) obtained by TEM from Ref. [46]. The miscut was $4°$. Films were grown by RF sputtering.

the magnetic films. More details on the preparation and magnetic properties of this kind of samples are found in Refs. [46, 72].

The magnetic domain structure in the FeNi layer was measured using XMCD-PEEM with the x-ray photon energy tuned to the Fe-L_3 absorption edge. The lateral resolution was set to 1 μm in this experiment. The PEEM and the measuring geometry used in this study is identical to the one described elsewhere [49]. The measurements were performed on beamline UE56/2-PGM2 of the synchrotron BESSY in Berlin.
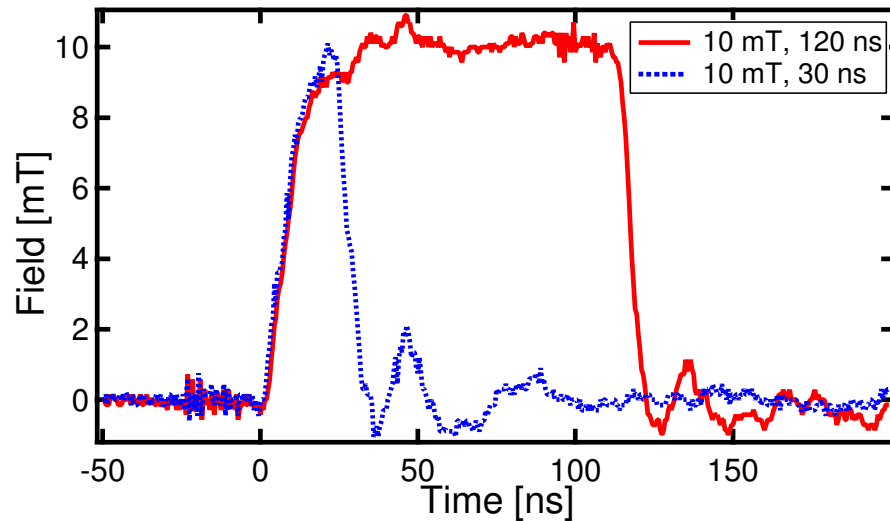

Figure 5.9: Shape of the magnetic field pulses. Solid and dotted curves correspond to 120 ns and 30 ns pulses, respectively. The amplitude of both pulses shown here is 10 mT.

5.2.2   Single-pulse experiment (1)

To study the magnetization reversal properties of the FeNi layer magnetically coupled to the Co layer (sample B), first both FM layers were saturated either in the same or in opposite directions. 1 ms-long, 30 mT magnetic pulses applied along the easy axis were strong enough to saturate both films, and a subsequent 4.5 mT-field reversed the magnetization of only the FeNi layer. 30 ns field pulses with various amplitudes were then applied to reverse the magnetization of the FeNi layer. The shape of these pulses is showed by the dotted line in Fig. 5.9. Images of the static magnetic domain structure were taken after the application of each magnetic pulse, so called single-pulse measurements. The ns-short magnetic field pulses with amplitudes between 3.3 and 16.3 mT were applied one by one to reverse the magnetization of the FeNi layer. Images of the magnetic domain structure were taken after application of each pulse, and the mobility of magnetic domain wall motion in the FeNi layer along the easy axis of magnetization (along the step-bunches on the

interfaces) was deduced. The reversal mechanism of the FeNi layer was found to depend on the applied pulse length, amplitude, and on the energy and direction of the coupling between the two FM layers.

In Fig. 5.10, the magnetization curve of the SV system obtained by quasi-static longitudinal Kerr effect measurements is shown by the grey solid line. A double step reversal being due to separate switching of the FeNi layer (lower H_C) and the Co layer (higher H_C) is seen. One of the two minor loops of the FeNi layer is also shown by the grey dashed curve, where the interlayer coupling is evidenced by the horizontal shift of the minor loop. The coupling energy, $\mu_0 H_{coupl}$, of about 2 mT is caused by correlated roughness at the two FM/Cu interfaces leading to a parallel coupling between two FM layers [70]. A localization of the coupling at the steps was found in the same type of sample [73].

The images in Fig. 5.11 (a) to (i) show the magnetic domain structure of the FeNi layer induced by 30 ns-short pulses (dashed curve in Fig. 5.9). The scale of the images is indicated on (e). First, both FM layers were saturated in parallel along the easy axis of magnetization, parallel to the step-bunches, by applying 30 mT field pulses of 1 ms duration with an external coil (Configuration A). Saturation was checked by XMCD-PEEM domain images. Magnetic pulses were then applied by
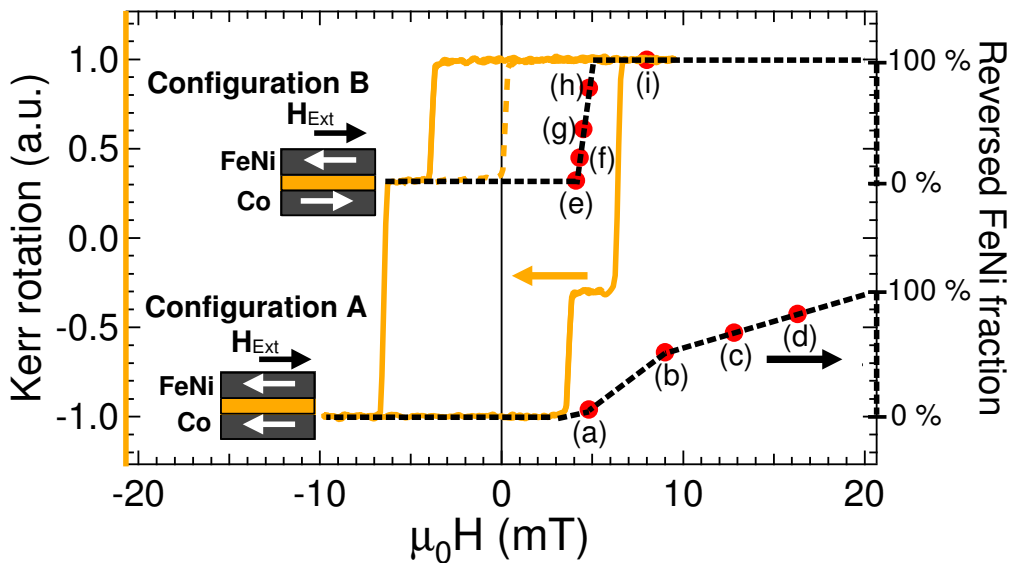

Figure 5.10: Hysteresis loop obtained by longitudinal Kerr effect measurements of the FeNi/Cu/Co trilayer (grey solid curve) in quasi-static conditions. One of two minor loops of the FeNi soft layer is also shown (grey dashed curve). The normalized Kerr rotation is labelled on the left axis. Circles show the fraction of reversed FeNi layer after application of 30 ns short field pulses, obtained from Fig. 5.11. Black dashed curves are guide to the eye. For these cases, the percentage of reversed area of the FeNi layer is given on the right axis.

the micro coil in the direction opposite to the magnetization directions of the FeNi and Co layers. PEEM image (a) was taken after application of 31 pulses of 4.8 mT. By applying these pulses, a white domain appeared from the left side of the image and propagated to the right. The direction of the field pulses and the magnetization directions of white and black regions are indicated by arrows. In general, domain wall motion as observed here is the predominant mechanism if the amplitude of the applied field is slightly higher than the coercive field, and also the zig-zag shaped domain wall is typical for head-on walls in films with uniaxial in-plane anisotropy [24]. Applying one 9.0 mT pulse after *re*-saturation of the films, also magnetic domain nucleation was observed and 55% of the image turned to white, as shown in Fig. 5.10 (b). The magnetic domain patterns (c) and (d) in Fig. 5.11 are after application of one 12.6 mT and one 16.3 mT pulse, respectively. One can see that the size of domains gets smaller and the number of nucleated domains becomes larger upon increasing the external field. Some of these domains were smaller than the lateral resolution, leading to an intermediate grey contrast. In summary, by increasing the pulse amplitude, a gradual transition of the reversal process from domain wall propagation to domain nucleation is observed. This leads to an increase of the number of domains, and a decrease of their average size with pulse amplitude.

In a second experiment, the two FM layers were initially saturated in opposite directions (Configuration B), and field pulses were then applied in the same direction as the Co layer magnetization. For single pulses, the magnetic fields needed to reverse the FeNi magnetization in Configuration B are much smaller than for Configuration A. In Configuration B, after one field pulse, domains were observed in a narrow range of fields, between around 4.0 and 8.0 mT. No white domains were observed after the application of one 4.1 mT field pulse (e). As increasing the amplitude of the field pulse from (f) to (g) to (h), the reversed area got larger, and the size of observed magnetic domains is larger, indicating that the domain wall propagation dominated the reversal. Totally white images (saturated) were observed with a 8.0 mT pulse. The percentage of the FeNi magnetization reversed in the PEEM images for different applied pulse fields is also plotted in Fig. 5.10, using the right axis. The dashed black lines are guides to the eye through the experimental points, indicating the FeNi hysteresis curve obtained for 30 ns-short field pulses for the two directions of the Co magnetization. The experimental points (a)–(i) are indicating the field amplitude of the pulses after which the corresponding images have been taken in remanence, and the corresponding permalloy magnetization. From Fig. 5.11 it is obvious that the FeNi reversal for switching parallel to the magnetization direction of the Co layer and antiparallel to it is quite different. This different behavior will be discussed in Section 6.3.

Config. A   **Config. B**

Hpulse

X-ray

70 μm

(a) 4.8 mT x 31   (e) 4.1 mT x 1

(b) 9.0 mT x 1   (f) 4.3 mT x 1

(c) 12.6 mT x 1   (g) 4.5 mT x 1

(d) 16.3 mT x 1   (h) 4.8 mT x 1
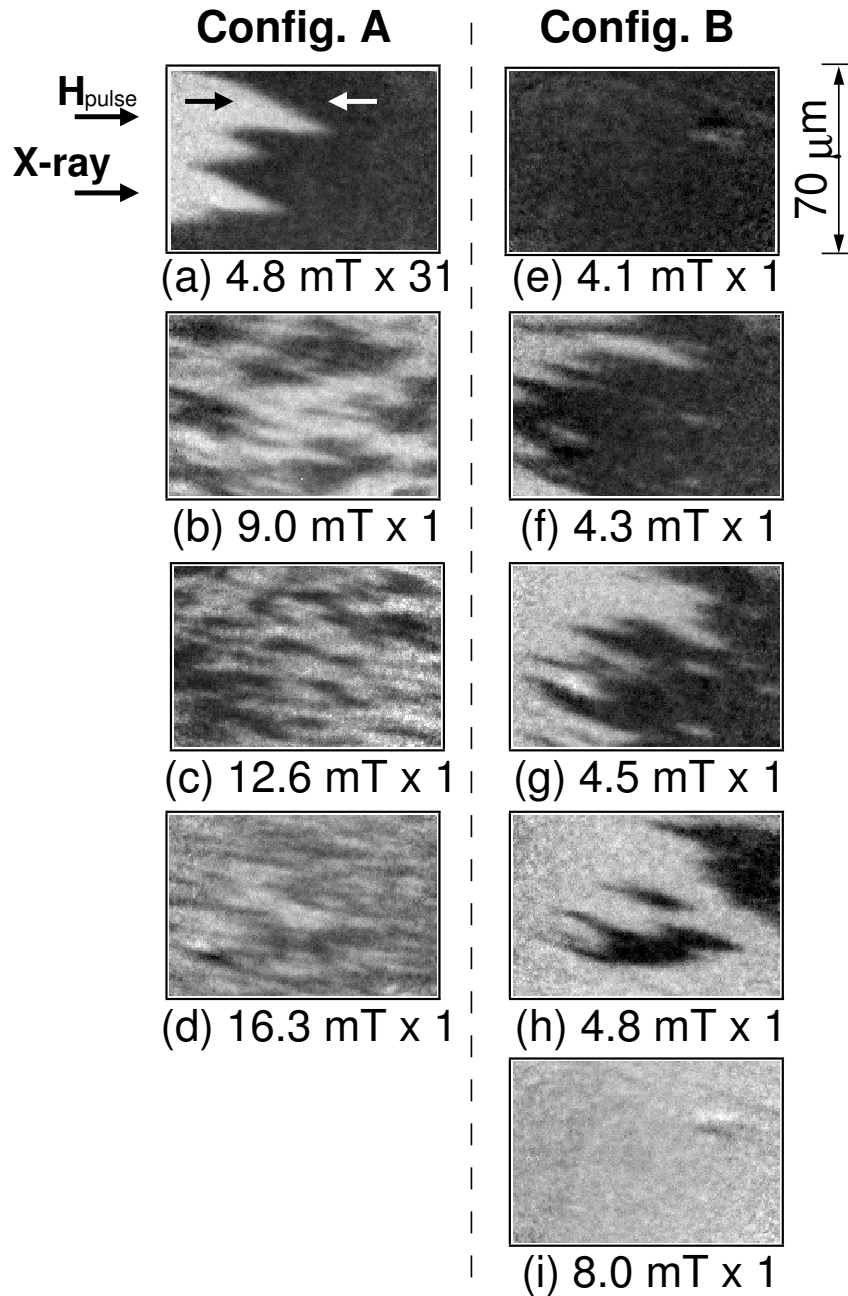
(i) 8.0 mT x 1

Figure 5.11: Images showing the magnetic domain structure of the FeNi layer obtained by XMCD-PEEM, where the photon energy of the circularly polarized x-rays was tuned to the Fe-L$_3$ absorption edge. Images were obtained after application of 30 ns-short field pulses. The number and amplitude of the pulses are written below each image. The initial configurations before application of the pulses for images (a)-(d) and (e)-(i) are A and B, respectively (cf. Fig. 5.10).

5.2.3 Single-pulse experiment (2)

Single-pulse measurements were also performed using 120 ns-short pulses with 10 ns rise- and fall-time (solid curve in Fig. 5.9). Panels (a) to (g) in Fig. 5.12 show the magnetic domain structure of the FeNi layer after successive application of 120 ns field pulses of identical amplitude. The field of view is 120 μm. Starting from Configuration A, pulses with amplitudes of 5.0 mT (i) and 6.1 mT (ii) were applied to reverse the magnetization of the FeNi layer. One 5.0 mT pulse created a small white domain at the middle of the image (a) which was probably nucleated at a surface defect. Then a second pulse was applied *without* re-saturation of the film, and a white zig-zag shaped domain appeared on the left side (b). The third pulse made the domain wall propagate to the right (c). Domain wall propagation was also observed when applying pulses of 6.1 mT (ii) and 3.3 mT (iii). In (iii), the direction of the external field was parallel to the Co magnetization (Configuration B). The magnetization of the Co layer was not influenced by the pulses with the amplitudes used here.

The speed of domain wall motion of the FeNi layer was estimated from these images in the following way. White circles were put onto the tips of white zig-zag domains in (b), (d) and (f), and crosses onto (c), (e) and (g). The circles were superimposed from (b), (d) and (f) to (c), (e) and (g), respectively. By taking the average displacement of the tips, the estimated speed of wall motion was 270 m/s, 410 m/s and 490 m/s for the three field pulses. In (ii) from (d) to (e), the shape of the domains was more or less preserved, but not in (i) and (iii). This leads to different errors in the domain wall velocity of ± 20 m/s for (ii) and (iii), and ± 80 m/s for (i). However, we can not exclude that some new domains nucleated between (d) and (e) since some small black domains are visible in the white region. In Configuration B, where the magnetization of FeNi reverses into the direction of the Co layer, faster wall propagation as compared with Configuration A was observed for a smaller field pulse amplitude. The domain wall motion obtained here was in the viscous regime or perhaps the wall motion above the Walker limit field, H_{Walker} (see Section 3.3), since the effective fields ($H_{eff} = H_{pulse} \pm H_{coup}$) were well above the coercivity of the FeNi layer and up to close to H_{Walker}, which is around 5 mT for FeNi derived from Eq. 3.26 taking $\alpha = 0.01$. Here H_{pulse} is the pulse field. However, an almost linear increase of the velocity was observed here, as will be explained in Section 6.7, and the mobility of wall motion can be derived from the slope of the plot of velocity as a function of H_{eff}.
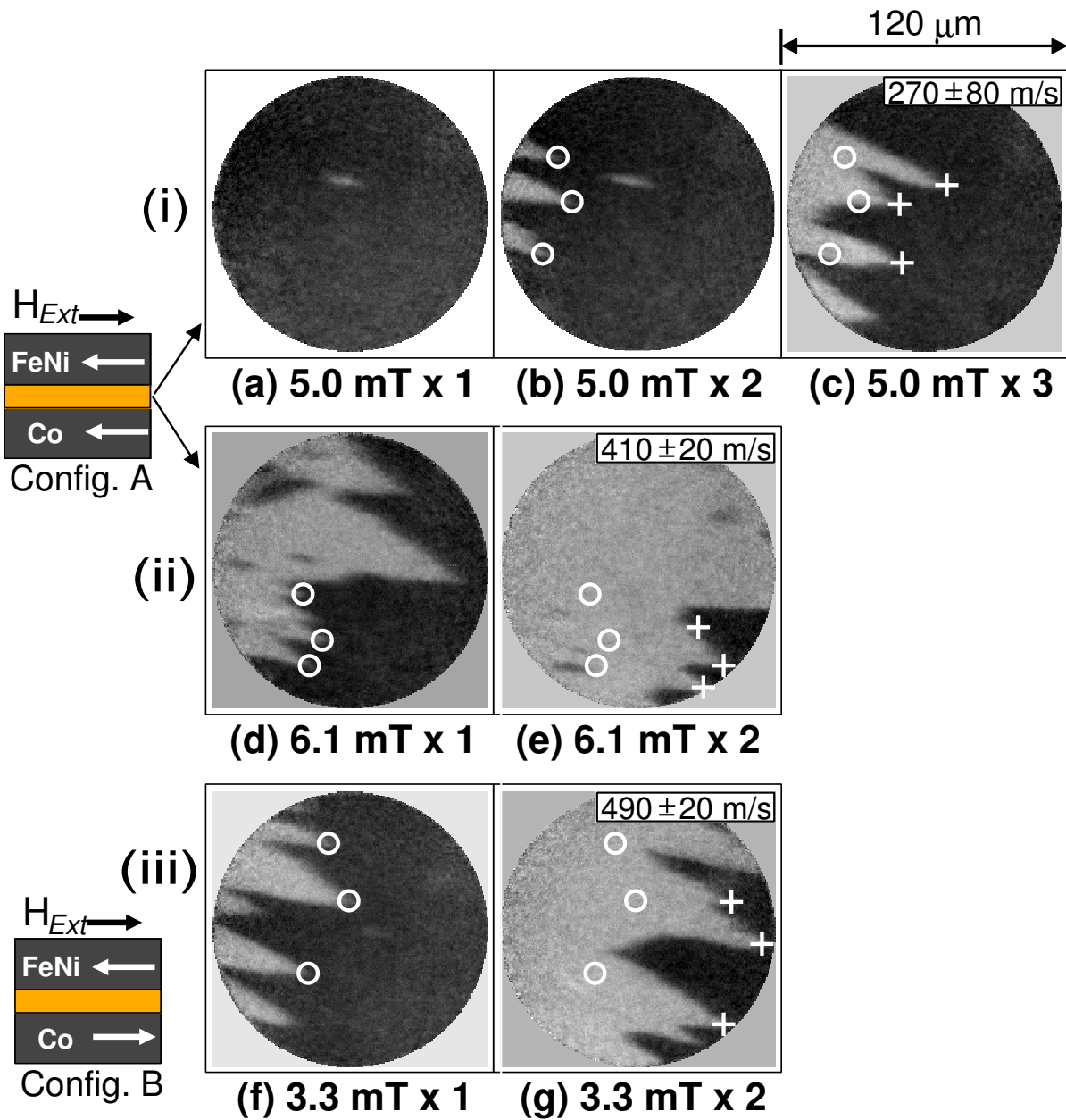
Figure 5.12: Magnetic domain structure of the FeNi layer. The field of view is 120 μm. First, the two ferromagnetic layers were either saturated in the same direction (Configuration A) or in opposite directions (Configuration B), then 120 ns-short magnetic pulses were applied to reverse the magnetization of the FeNi layer. Images were taken after each pulse without re-saturation of the films, in order to visualize the progress of the domain walls. The number and amplitude of the applied pulses are written below each image. White circles were used to mark the tips of white zig-zag domains in (b), (d) and (f), and crosses in (c), (e) and (g). The circles were superimposed from (b), (d) and (f) to (c), (e) and (g), respectively. The average distance between circles and crosses was used to estimate the domain wall velocity.

5.3 Non reproducible domain wall motion

5.3.1 Sample C

In Fig. 5.13, the structure of the SV-like sample C is shown. The trilayer, 5 nm $Fe_{20}Ni_{80}$/4 nm Cu/8 nm Co, capped with 3 nm of Al, was grown by RF sputtering on SiO/Si(100). The in-plane uniaxial magnetic anisotropy was induced by applying a magnetic field during the growth. The Kerr loops along the easy axis of magnetization are shown in Fig. 5.14, and the loop obtained along the hard axis is in the inset. The field induced anisotropy energy is explained in Section 2.3.3. The two-step magnetization reversal in Fig. 5.14 indicates that the FeNi and Co layers have a lower and a higher H_C, respectively. The minor loops from the FeNi layer, drawn by the dotted curves, are shifted about 0.4 mT from being symmetric to zero field due to the coupling field from the Co layer.

The pump-probe and single-pulse experiments have been performed with bipolar pulse fields at the beamline UE56/2-PGM2 in BESSY. A non-reproducible magnetic domain wall motion by magnetic pulses was observed.
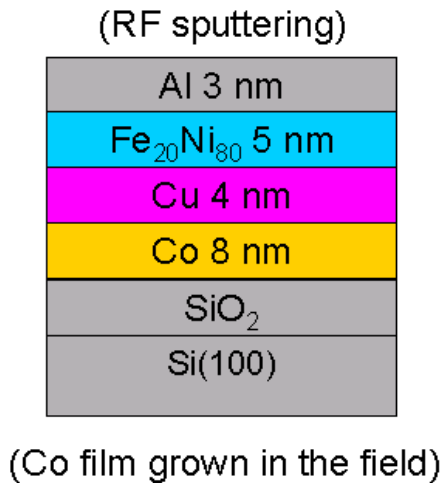

Figure 5.13: Scheme of sample C. The SV like trilayer with the Al capping layer is grown by RF sputtering on a SiO/Si(100) surface. A uniaxial anisotropy was induced by the deposition in the field. The anisotropy axis is along the applied field direction.
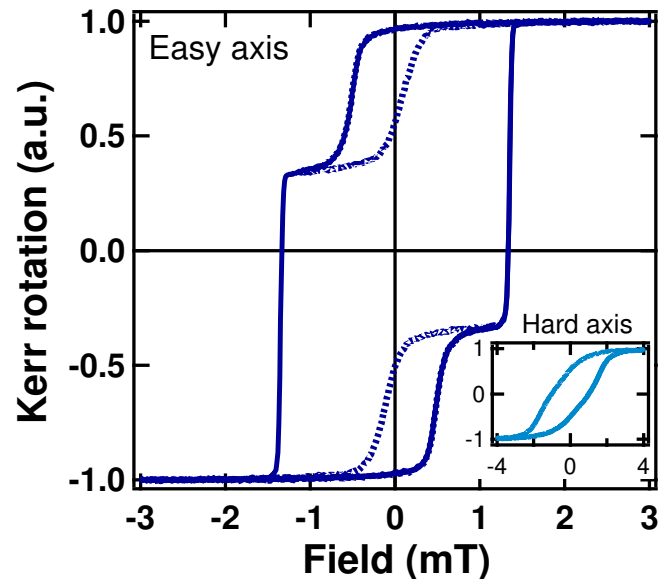
Figure 5.14: Longitudinal magnetic hysteresis loops along the easy axis are shown, and the loop along the hard axis is in the inset. The two step magnetization reversal indicates the different H_C of the FeNi (low) and Co layer (high). Two minor loops from the FeNi layer are plotted by the dotted curves. They are shifted by 0.4 mT due to the coupling to the Co layer.

5.3.2   Pump-probe experiment

Time-resolved stroboscopic XMCD-PEEM experiments were performed on the sample C (Fig.
5.15). Domains were initially induced in the Co layer using 3 ms-long pulses from an external
coil as a starting configuration. The domain structure in the Co layer is shown in (d), and its
magnetization was not affected by the bipolar magnetic field pulses. The shape of the bipolar
pulses is shown in (e). The amplitude of the field pulse was 1 mT at maximum for both polarities,
and the length was 60 ns. The magnetic domain structure in the FeNi layer at different delay times,
before the pulse and at the maximum of the first positive and the second negative pulses, is shown
in (a), (b) and (c), respectively. The easy axis of magnetization is running parallel to the vertical
direction in the images, and the field of view is 100 μm. The field directions of the first positive
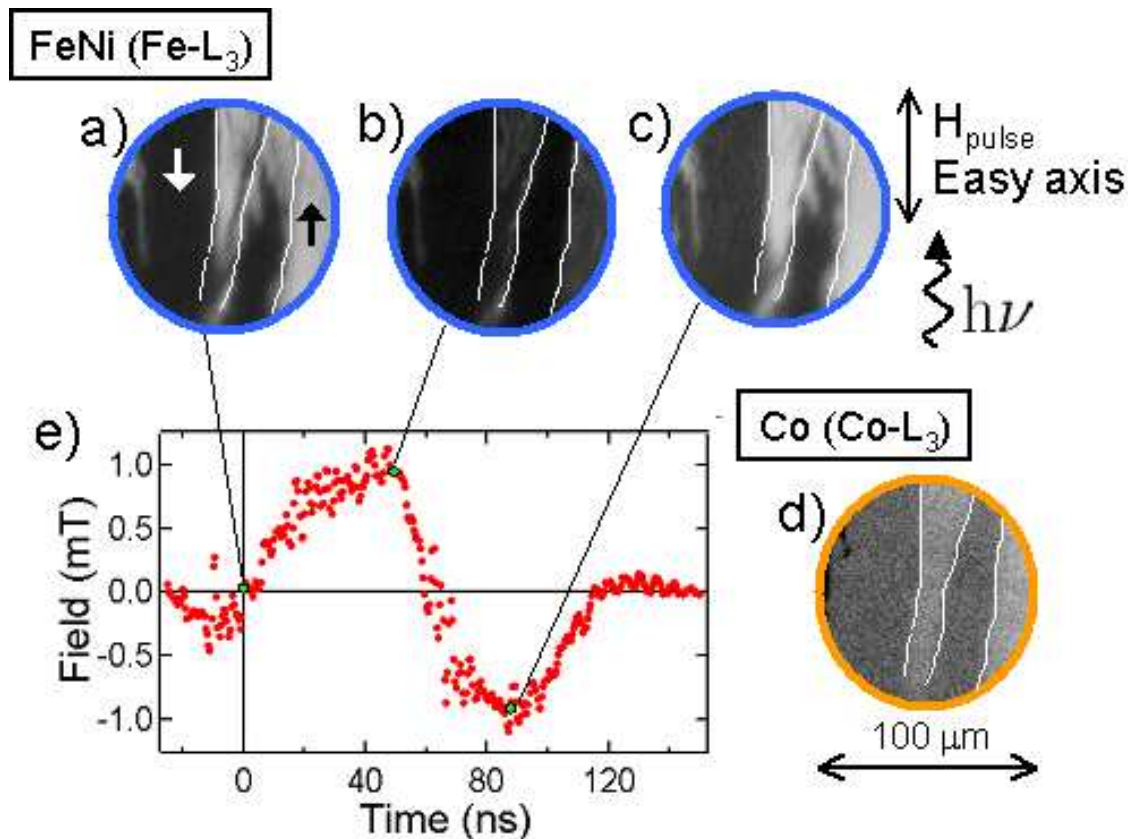

Figure 5.15: Time- and layer-resolved XMCD-PEEM domain images of the FeNi layer at different
pump-probe delay times (a – c). The magnetization in the Co layer (d) was not affected by the field
pulses. White lines in (d) that mark the position of the domain walls were superimposed to the
FeNi images. The field of view is 100 μm. The shape of the bipolar magnetic field pulse is shown
in (e). The field amplitude was 1 mT for the positive and the negative pulses, and the length was 60
ns.

and the second negative pulses are down and up, and they make the image darker and brighter, respectively.

For all three images of the FeNi layer, one can see a correlation of the domain structure to the one of the Co layer, induced by the magnetic interlayer coupling. During the first pulse, where the direction of the field is the same as dark contrast magnetization, the FeNi layer shows some fuzzy dark grey contrast (b) in the region in which the Co has white domains. During the second pulse (c), the area where the Co layer has white domains is almost saturated by white domains in the FeNi layer, however, there are also some fuzzy dark grey domains in the dark contrast regions between the two white stripe domains, and at the left side of the image. These fuzzy grey contrasts indicate that dark (white) domains existed in the FeNi layer in the region where the Co layer exhibits white (dark), but not for every pulse, meaning that the wall motions are not reproduced for every magnetic pulse.

5.3.3 Single-pulse experiment

To confirm the non-reproducibility of the wall motion for each field pulse, single-pulse experiments were performed (Fig. 5.16). A single domain wall was created in the Co layer by the external coil (e). The magnetic pulse used for this experiment, shown in (a), is similar to the one used for the pump-probe experiment described above, with a maximum amplitude of 1 mT for both the first and the second pulse, and a length of 60 ns. The magnetic field pulses were applied one by one, and the domain structures were recorded after every pulse in static conditions. They are shown in Fig. 5.16 (b), (c) and (d). It is clearly seen that for each image the domain structures are different. On the right hand side of the images, where the Co layer has a white domain, there are $360°$ domain walls (thin black lines) in the FeNi layer, and they are moved by the field pulses. This may lead to the observed fuzzy grey contrast in Fig. 5.15. The connection between reproducibility and magnetic anisotropy energy will be discussed in Section 6.4. In the dark area of the Co layer, close to the domain wall, always dark domains exist in the FeNi layer with around 15 μm width. It seems that the stray field from the domain wall in the Co layer affects the magnetization in the FeNi layer. In Section 6.8, the influence of the stray field on the magnetization of the FeNi layer in sample E is discussed.
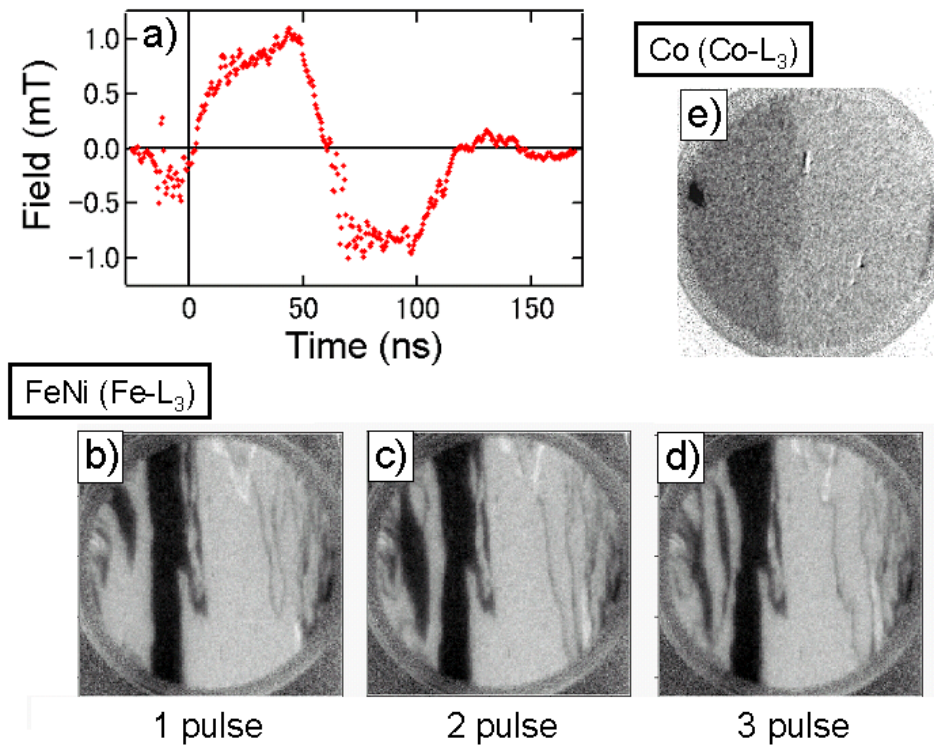
Figure 5.16: Single-pulse experiments performed on sample C. The domain structures in the FeNi and the Co layers are shown in (b – d) and (e), respectively. The images for the FeNi layer show different domain structures after application of each identical pulse, indicating that the wall motions are not the same for each pulse.

5.4 Magnetization reversal on a weak anisotropy trilayer

5.4.1 Sample D

The SV-like sample (Fig. 5.17), 5 nm $Fe_{20}Ni_{80}$/4 nm Cu/5 nm Co capped with 3 nm of Al, was grown by RF sputtering on a SiO/Si(100) substrate. It is almost the same as the sample C, only the Co layer is thinner. For the magnetic properties, H_C of the two FM layers and H_{coup} (where $\mu_0 H_{coup}$ = 0.4 mT) are almost the same as in the sample C. However, the films were grown in zero external field, so that the films have a negligible magnetic anisotropy in the film plane. Kerr loops obtained in different in-plane angles showed a similar shape to the loop in Fig. 5.18. The two minor loops from the FeNi layer are drawn by the dotted curves.

From the tilted and more rounded hysteresis loop of that shown in Fig. 5.18, one can guess that the magnetization reversal does not only take place by domain wall motion but also by the nucleation of small domains. Because of this reason, the beamline UE52-SGM in BESSY is used, in which the synchrotron x-rays are horizontally focused at the measurement position to 35 μm. The higher flux density of photons compared to the UE56/2-PGM2 beamline allowed to set the instrument to a higher lateral resolution. The pump-probe experiments were performed with monopolar
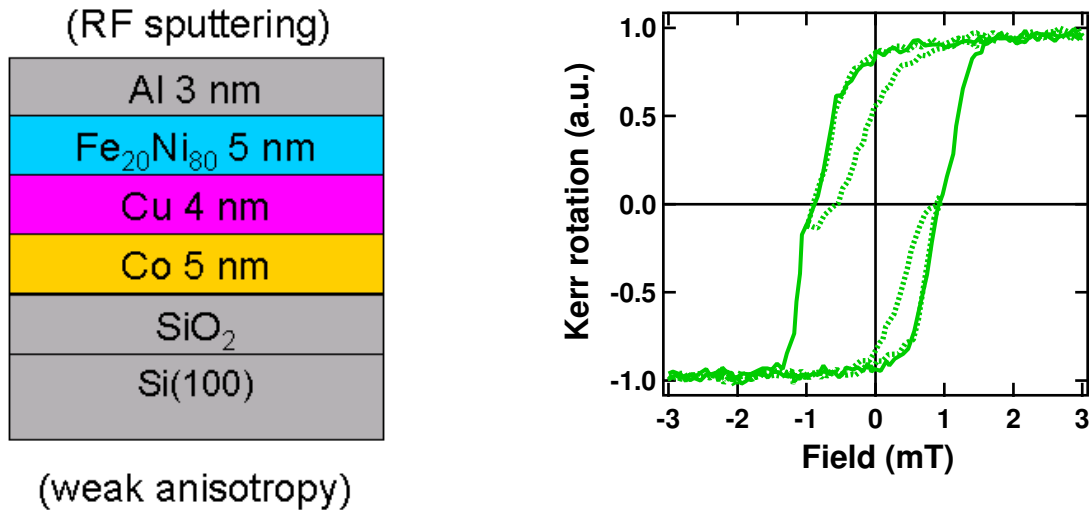

Figure 5.17: Scheme of sample D. The SV like trilayer was grown by RF sputtering on a SiO/Si(111) surface in static conditions. The layer structure is similar to sample C, but the thickness of the Co layer is a bit thinner.

Figure 5.18: Longitudinal Kerr effect measurements show that the loops have similar shapes in different azimuthal field directions, indicating that the films had an almost negligible anisotropy in the film plane. The two step magnetization reversal is more smeared out in that sample, but nevertheless indicates that the FeNi (low) and Co (high) layer have different H_C. Two minor loops from the FeNi layer are plotted by the dotted curves. They are shifted by 0.4 mT due to the coupling field from the Co layer.

pulse fields. A high reproducibility of the wall motion was observed, which is one of the quite
different properties compared to sample C.

5.4.2 Pump-probe experiment

Magnetization dynamics of the FeNi layer in sample D, which has a negligible anisotropy in the
film plane (see Figs. 5.17 and 5.18), was studied using focused circularly polarized x-rays. This
high flux photon pulse allowed to increase the lateral resolution to ∼150 nm. Magnetic monopolar
pulses with a maximum field strength of 4.5 mT, duration of 18 ns, and 5 ns rise time were used. The
pulse shape is displayed in Fig. 5.19 (f). The pulse shape was determined from the displacement
of the PEEM image perpendicular to the field direction, as explained in Section 4.2. Fig. 5.19 (a)
- (d) show the magnetic domain structures in the FeNi layer at different delay times. The domain
structure in the Co layer, shown in (e), was not affected by the field pulses. The grey contrast
is small, because the Co layer is buried by 12 nm of other material. However, it is possible to
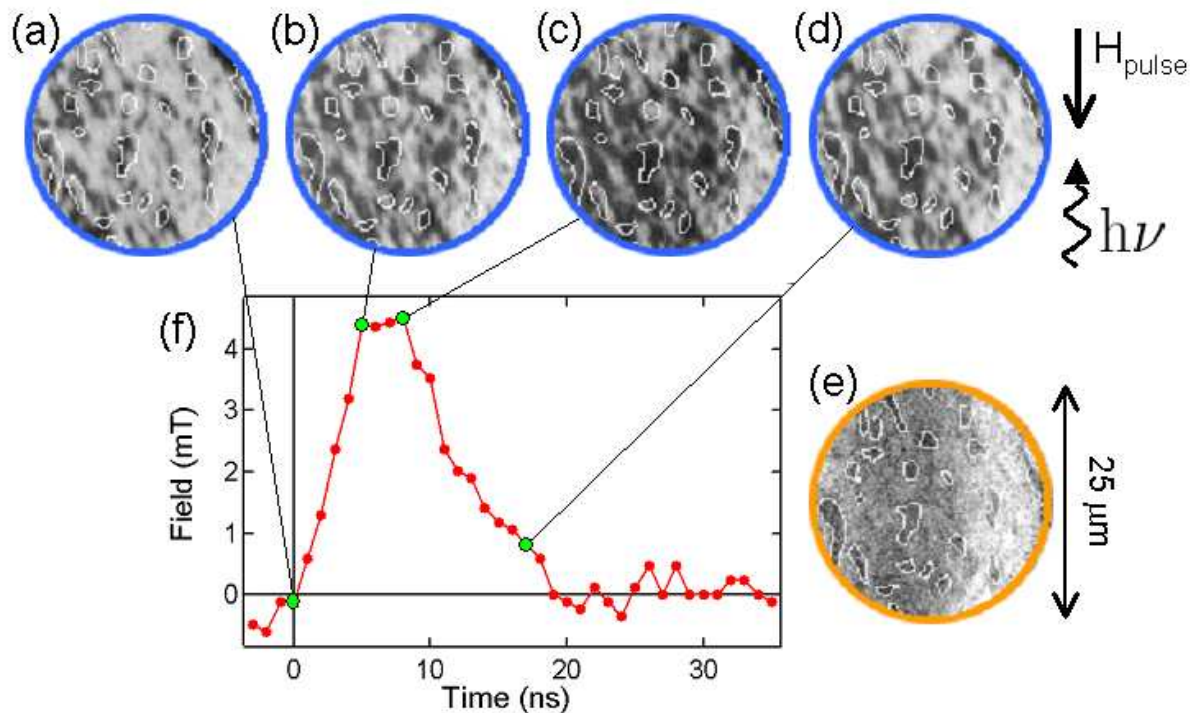recognize where magnetic domains exist in the Co layer. They are indicated by white lines in (e).

Figure 5.19: Magnetic domain structures in the FeNi layer (a - d) obtained by stroboscopic pump-
probe experiment at different times before, during, and after the magnetic field pulses (f), as in-
dicated by lines. Image (e) shows the magnetic domain structure of the Co layer, which was not
affected by the magnetic field pulses.

The white lines are superimposed to images (a) to (d). The field of view is 25 μm in diameter. It is seen that the domain structure in the FeNi layer, before the pulse (a), is similar to the one in the Co layer, but not identical. The dark and bright domains correspond to magnetization pointing down and up in the images, respectively. The field pulse direction is parallel to the magnetization of the dark domains. The surface fraction covered by dark domains increases from (a) to (b) to (c) mainly by the expansion of existing dark domains. The magnetic domains shown here are smaller and more irregularly shaped than in sample C, even though the two samples have similar layer structures. The difference is that sample C has a uniaxial magnetic anisotropy energy while sample D is nearly isotropic.

Interestingly, the dark domains already start to shrink when going from (c) to (d), while the external field is still in the "dark" direction. This has to be attributed to the coupling to the Co layer
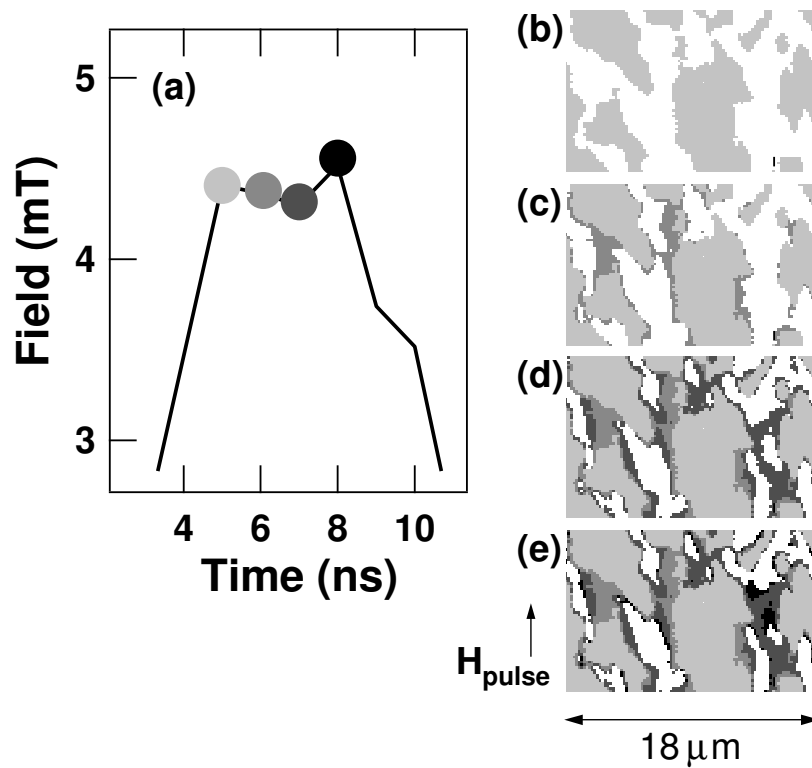

Figure 5.20: (a): Magnified view of the maximum of the magnetic field pulses. (b) – (e): Analysis of switching by expansion of domains, extracted from differences between discretized layer-resolved magnetic domain images of the FeNi layer acquired every 1 ns during the plateau of the field pulse. Differently grey shaded areas correspond to reversed domains present in the FeNi layer after the time delays indicated in (a) i.e., (b) 5 ns, (c) 6 ns, (d) 7 ns, and (e) 8 ns.

in the regions where the Co magnetization is along the "white" direction. This coupling and a small overshoot of the field pulse at around 20 ns always bring the magnetic domain structure back to the starting configuration (a). The grey contrast of stroboscopic images shown in Fig. 5.19 and images obtained in static conditions is almost the same, which indicates that the wall motion observed here is repeated identically for almost every magnetic field pulse.

The maximum of the field pulse features a 3 ns wide plateau where the field is almost constant (Fig. 5.19 (f)). Here, information on the magnetization reversal dynamics at a constant field can be separated from the influence of changing the external field. Fig. 5.20 shows a detailed analysis of the dynamics of domain expansion during that time. Panel (a) presents a blown up view of the maximum of the field pulse. The magnetic domain structure in the FeNi layer has been acquired at 5, 6, 7 and 8 ns delay time, as marked by symbols of different grey shade. (b) – (e) show how the reversed domains expand as a function of time at those four delays. Bright grey areas correspond to regions in which reversed domains already existed at 5 ns. Image (b) thus represents a discretized version of Fig. 5.19 (b). Areas plotted in different darker shades of grey in subsequent panels correspond to the times indicated by the symbols of the corresponding shade of grey in Fig. 5.20 (a). The biggest changes, i.e., the largest intermediate and darker grey areas in Fig. 5.20 (e), are seen in regions where two existing domains are getting connected. In these areas, the evolution of reversed domains is somehow reminiscent of merging water droplets. One of this behaviors is seen, for example, on the left side in (c). The two magnetic domains shown by light grey contrast get connected with a domain with a darker grey. The domain wall velocity can be estimated from Fig. 5.20, and is as high as 1 μm/ns where two domains get connected. In general, domain wall velocities extracted for domains that do not connect are much lower, and the propagation within 3 ns is comparable to the lateral resolution.

5.5 Magnetization reversal by nucleation and propagation

5.5.1 Sample E

The sample E contains a 4 nm $Fe_{20}Ni_{80}$/2 nm Al_2O_3/7 nm Co MTJ like trilayer, which was grown by RF sputtering on a step-bunched Si(111) surface (Fig. 5.21). Underneath the Co layer, 3 nm of CoO has been deposited to increase H_C of the Co layer. The NiFe layer has been capped by 3 nm of Al layer to prevent oxidation. The details of the thermal treatment to create step-bunches are introduced in Section 5.2, and also in Ref. [72]. The miscut of this sample is $6°$ along the $[\bar{2}11]$ crystal axis. According to the longitudinal Kerr effect experiments (see Fig. 5.22), the sample has a uniaxial anisotropy along the step-bunches. The two-step magnetization reversal indicates that H_C of the FeNi (lower) and the Co (higher) layers are different. The loop-shift of the two minor loops from the FeNi layer indicates that the two FM layers are magnetically coupled ($\mu_0 H_{coup} = 1.2$ mT). The details of similar types of samples are shown in [16–18, 46, 74].

The PEEM used here is from Focus Gmbh (Fig. 4.3), and the excitation source was the twin helical undulator beamline UE56/2-PGM2 in BESSY. Using the XMCD-PEEM with a pump-probe technique, the nucleation of domains and the subsequent wall motion in the viscous regime up to the saturation of the velocity could be observed on a plateau of the ns-long magnetic field pulses.

Furthermore, at exactly the same position on the sample surface, a mechanism of magnetic
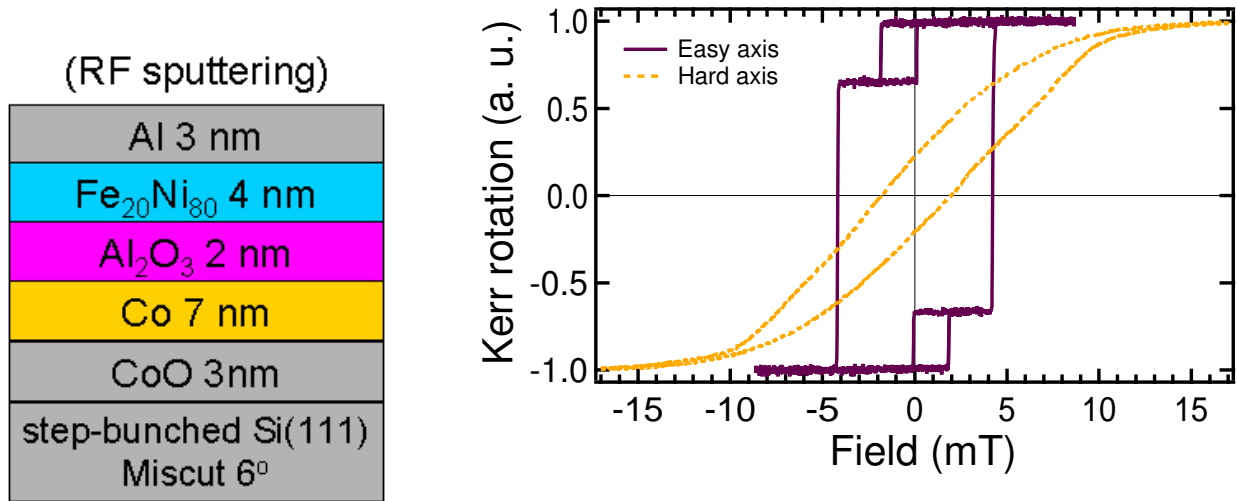

Figure 5.21: Scheme of sample D. The MTJ like trilayer was grown by RF sputtering on a step-bunched Si(111) surface. The miscut was $6°$.

Figure 5.22: Magnetic hysteresis loops for the easy axis (solid curve) and hard axis (broken curve) are shown. The easy axis is along the step-bunches on the sample surface. Two-step reversal indicates that the coercivity of the FeNi layer (low) and Co layer (high) are different. The minor loops from the FeNi layer are shifted left or right from the zero field position by the coupling energy (coupling field = 1.2 mT).

domain nucleation has been studied. Interestingly the stray field from the wall in the Co layer initiated the domain nucleation in the FeNi layer. Spins in the FeNi layer above the wall were nearly 90° tilted by the stray field, resulting in a drastic reduction of the nucleation field in this region.

5.5.2   Pump-probe experiments

Sample E shows a more squared magnetic hysteresis loop (see Fig. 5.22) compared to the ones from the samples C and D. It may indicate that the magnetization reversal takes place predominantly by magnetic domain wall propagation rather than by domain nucleation, suggesting that the number of nucleation centers in sample E is smaller than in samples C and D. To observe the nucleation of domains and the subsequent domain wall motion in dynamic experiments, the magnetic pulse power supply had to be improved to have long plateaus and shorter rise-times.

Two kind of micro-magnetic properties acting on the magnetization reversal in the FeNi layer are observed by the stroboscopic pump-probe experiment.

- Magnetic domains are nucleated and expanded during the plateau of the field pulses. The observed velocity of wall motion was in the viscous regime up to the saturation of velocity. A time delay of domain expansion depending on the amplitudes of the field pulses was observed, which can be fully understood by considering the domain wall energy.

- A domain nucleation in the FeNi layer initiated by the magnetic stray field from the domain wall in the Co layer has been observed.

Domain nucleation and the subsequent expansion

XMCD-PEEM experiments with the pump-probe technique were performed on the sample E. In Fig. 5.23, the nucleation of domains and their subsequent expansion in the FeNi layer obtained for a certain amplitude of bipolar field pulse are presented. The shape of the bipolar pulses is shown in (e). Both the positive and negative parts of the pulses have the same amplitude (5.80 mT) and the same length (45 ns). (a), (b), (c) and (d) are the magnetic domain structures in the FeNi layer at different pump-probe delay times, 11, 21, 26 and 31 ns, respectively. The starting of the positive pulse is set to zero time, and the plateau of the pulse starts at 11 ns, at which time still no domains are visible (a). The black and white contrasts indicate that the magnetization points down and up, respectively, in the images. The easy axis is running parallel to the vertical direction in the images, and the direction of incoming x-rays with 30° grazing angle is also indicated in (d). The field of view is 120 μm in diameter.
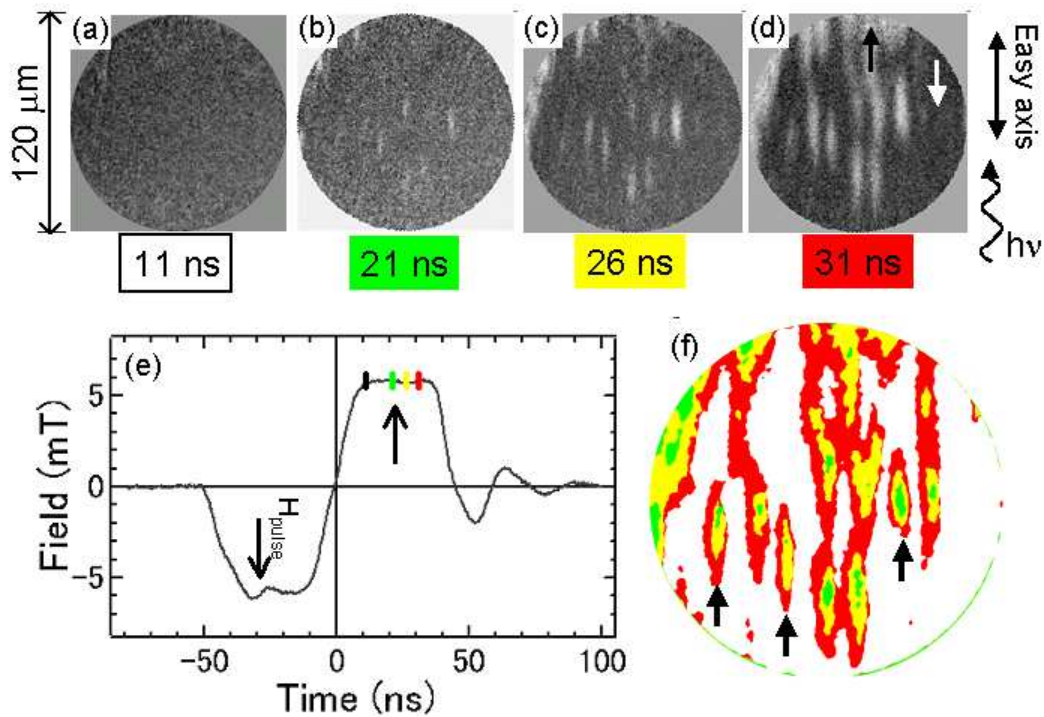
Figure 5.23: Bipolar magnetic field pulses (e) were used to reverse the magnetization in part of the FeNi layer. The amplitude of the field pulses was 5.80 mT on both the plateaus of the positive and negative part of the pulses. The magnetic domain structures in the FeNi layer at different delay times is shown in (a – d), where the photon energy of circularly polarized x-ray was tuned to the Fe-L_3 absorption edge. White domains in (b) to (d) are discretized and superimposed to (f). Different shades of grey show different delay times. It was confirmed from images taken at the Co-L_3 edge that no magnetization changes in the Co layer.

Before applying the pulses, the two FM layers were magnetically saturated in the same direction by a 15 mT field pulse of 3 ms duration. The direction is indicated by a white arrow in (d), and it shows black contrast. On the pump-probe experiments, the first negative pulse is the same direction as the saturation, and the second positive pulse is opposite (see (e)). The latter starts to reverse the magnetization in the FeNi layer. Some white domains become visible in (b), and as time goes by they get bigger (c and d). The first negative part of the pulse, every time, saturated back the FeNi layer by a great help of the coupling field ($\mu_0 H_{coup} = 2.0$ mT). To get enough statistics, millions of pulses were applied to acquire one image. Since the image contrasts shown here and the one obtained in static conditions are almost the same, the domain nucleation and the wall motion are reproduced on almost every field pulse.

The areas of white domains in (b), (c) and (d) are superimposed into (f) with different shades of grey, middle grey, light grey and dark grey, respectively. The expansion of the domains by
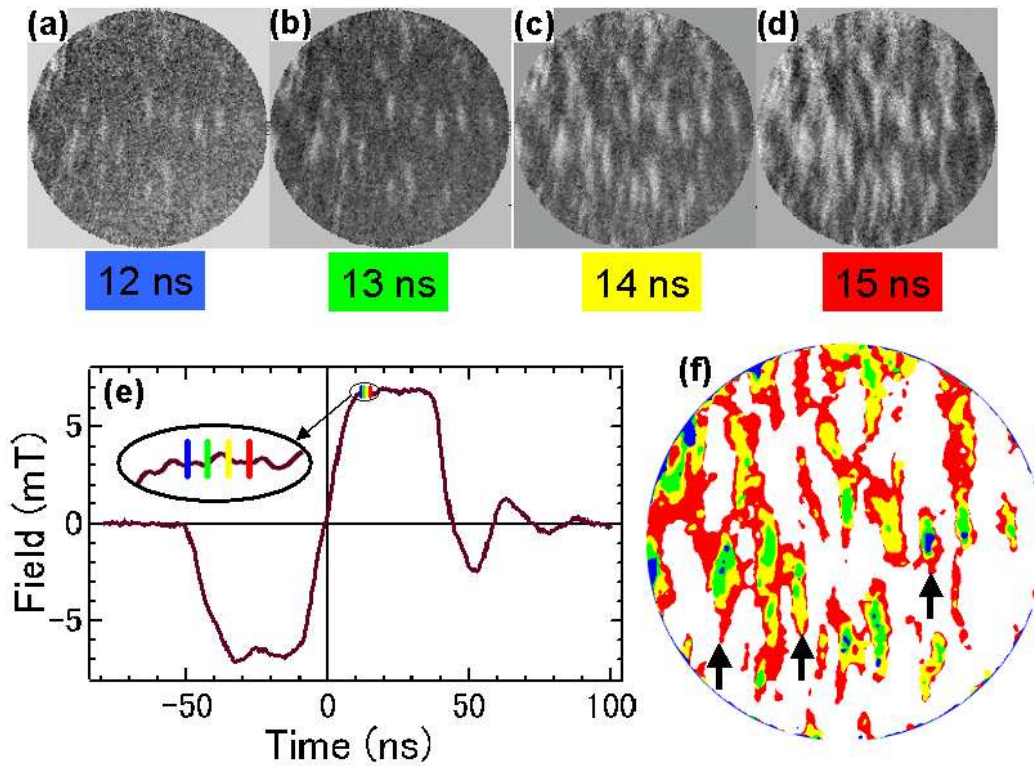
Figure 5.24: Same experiment as Fig. 5.23, but for a field amplitude of 6.81 mT.
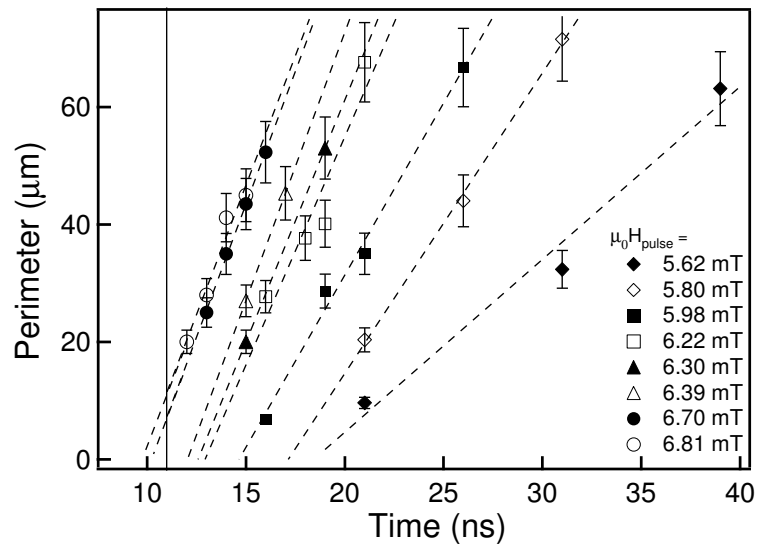

Figure 5.25: Average perimeter of three domains (indicated by arrows in Fig. 5.23 (f) and 5.24 (f)) vs. time. The expansion of the perimeter was observed on the plateau of the second, positive, part of the pulses for every amplitude of the field pulses, ranging from 5.62 mT to 6.81 mT. Broken lines are linear fits to the data.

propagation of the domain walls is clearly seen. In this experiment, the magnetization of the Co layer was not affected by the field pulses, i.e., it always showed the black contrast.

One more example is shown in Fig. 5.24, which was obtained with the strongest field pulse (6.81 mT) used in this experiment. The observed wall motion is much faster, and the number of nucleated domains is larger than the one shown in Fig. 5.23. Some domains are already visible at 12 ns (a), which is 1 ns after the starting of the plateau. Domain expansion is clearly seen every 1 ns time increment. All the shapes of the bipolar field pulses used in this study and all XMCD-PEEM images used for the following analysis are shown in the Appendix.

In Fig. 5.25, the average perimeter of three domains indicated by arrows in Fig. 5.23 (f) and also in Fig. 5.24 (f) is plotted as a function of time for all amplitudes of the field pulse, H_{pulse}, where $\mu_0 H_{pulse}$ is ranging from 5.62 mT to 6.81 mT. The three domains were nucleated for all amplitudes of the field pulses, and it was possible to measure their perimeter before they merged to other surrounding domains. Furthermore, all motions were successfully observed on the plateau of the field pulse. There is an error of 10% in the estimation of the perimeter. The plateau of the field pulses starts at 11 ns, indicated by a vertical line in Fig. 5.25. Linear fits to the data (broken lines) indicate that the perimeter of the domains extended linearly with time for each field amplitude. However, the intersections to the time axis of these lines do not come to the same point. It becomes smaller upon increasing the pulse field. There seems to be a delay of domain expansion.

Domain nucleation on the wall

Another time-resolved XMCD-PEEM experiment was performed at the same sample position as the above experiment shown in Section 5.5.2, however, now a domain was introduced in the Co layer as an initial condition. The domain structure in the Co layer is shown in Fig. 5.26 (h). The pulse field was kept such that it did not modify the domain structure in the Co layer. The pulse shape is shown in (i), the field amplitude was around 6 mT and the length was around 45 ns for both positive and negative parts of the pulses. The magnetic domain structures in the FeNi layer for different pump-probe delay times are shown in (a) – (g). The field of view is 120 μm in diameter, and the x-rays came to the sample from the bottom of the images with 30° grazing incidence angle. The easy axis of magnetization (step-bunches) is running vertically. The white area in the images shows magnetization pointing up and the dark area down, as indicated in (a). The direction of the positive and negative field pulses were down and up in the images, respectively, meaning that the first negative pulse tends to expand the dark domains, and the second positive pulse the white
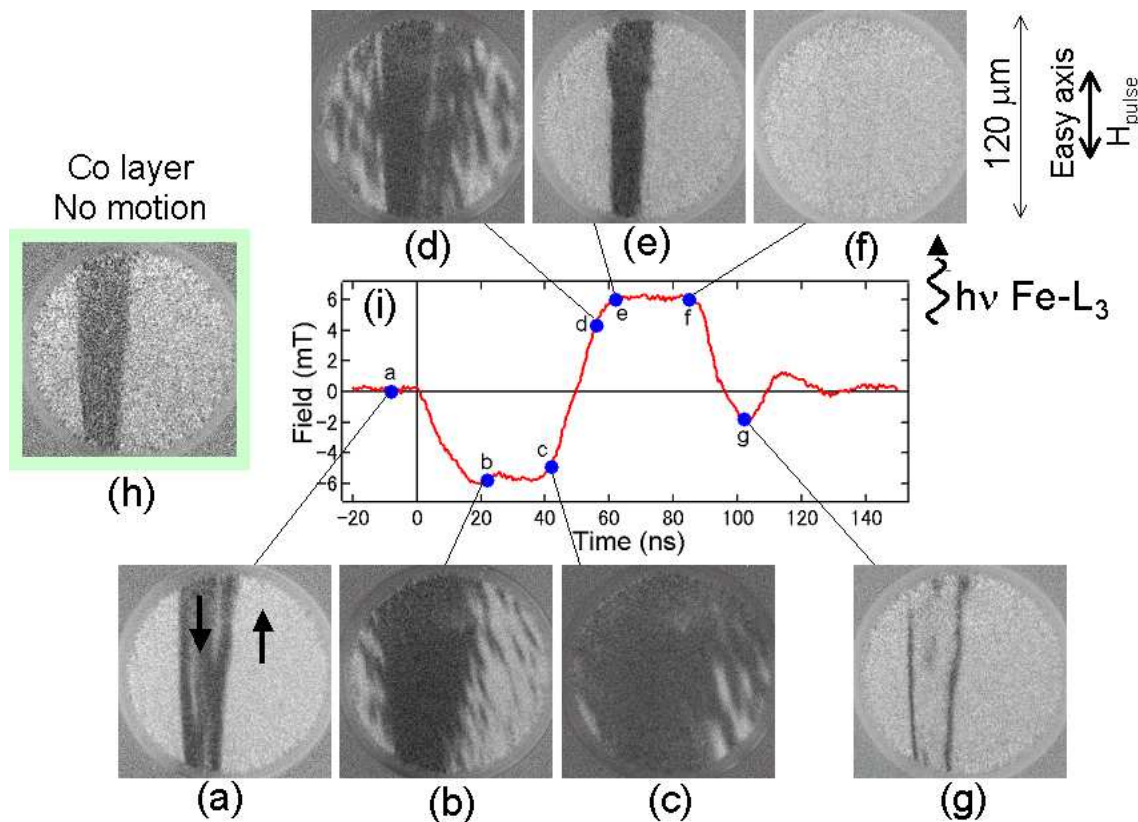

Figure 5.26: Domain structure in the FeNi layer at different pump-probe delay times (a to g). The domain structure in the Co layer (h) was not affected by the magnetic pulse field. The pulse field amplitude was 6 mT for both polarizations with a length of 45 ns.

domains.

Before the pulse (a), the domain structure in the FeNi layer is similar to that of the Co layer, but some line-shaped white domains are seen in the dark region. On the negative pulse, dark domains propagate from the wall to both sides, but also nucleation of some dark domains is seen (b). When the magnetization of the FeNi layer reversed against the Co layer magnetization, the domain wall motion was suppressed and the nucleation of domains was dominant. It was also observed in Section 5.2. At almost the end of the negative pulse, the FeNi is nearly saturated within the field of view (c). On the positive part of the pulse, the white domains come back into the field of view mainly by domain wall propagation, however, interestingly, two nucleated white line-shaped domains are seen, which are exactly at the position of the wall in the Co layer (d). It seems that the nucleation of domains is initiated by the wall in the Co layer. As time goes by, the FeNi layer shows almost the same domain pattern as the Co layer (e), and at the end of the pulse it is almost saturated (f). But indeed, there are faint grey line-shaped domains at the position of the wall in the Co layer. These are almost invisible, but they are enhanced by the negative overshoot of the pulse (g), which shows that they act as nucleation center for the reversal of the FeNi layer.

The mechanism of magnetic domain nucleation is still unknown. It is said so far that the nucleation of domains takes place on topological defects where the torque of magnetization by the external field is high, because in such regions spins point randomly. The nucleation of magnetic domains in the FeNi layer at the position of the domain wall in the Co layer observed in this study was systematically understood and discussed by considering the stray field from the wall in the Co layer (Section 6.8).